NANO LETTERS

LETTER

pubs.acs.org/NanoLett

Low Temperature Raman Study of the Electron Coherence Length near Graphene Edges

Ryan Beams,[†] Luiz Gustavo Cançado,[‡] and Lukas Novotny*[,†]

[†]Institute of Optics, University of Rochester, Rochester, New York 14627, United States

[‡]Departamento de Física, Universidade Federal de Minas Gerais, Belo Horizonte, MG 30123-970, Brazil

ABSTRACT: We developed a novel optical defocusing method for studying spatial coherence of photoexcited electrons and holes near edges of graphene. Our method is applied to measure the localization l_D of the disorder-induced Raman D band ($\sim$1350 cm^{-1}) with a resolution of a few nanometers. Raman scattering experiments performed in a helium bath cryostat reveal that as temperature is decreased from 300 to 1.55 K, the length l_D increases. We found that the localization of the D band varies as $1/T^{1/2}$, giving strong evidence that l_D scales with the coherence length of photoexcited electrons near graphene edges.

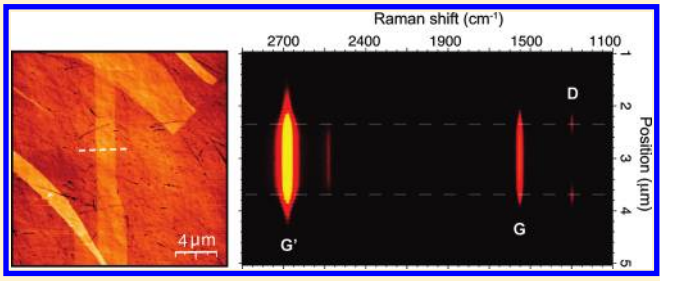

KEYWORDS: Graphene, optical properties, Raman scattering, spectroscopy, defects, localization

Over the past decades, silicon based materials spurred the development of ever smaller and faster transistor devices and the production of ever larger information storage. However, as the material dimensions become comparable to the length scale of electronic wave functions, it is necessary to explore alternative materials with enhanced performance. Low-dimensional carbon materials, such as carbon nanotubes and graphene, form a particularly promising alternative to silicon-based materials.[1,2] Monolayer graphene exhibits unique electronic transport properties, such as high electron mobility at room temperature and large tunable carrier densities.[3] These properties have led to extensive research and motivated the development of proof-of-concept devices, such as single electron transistors (SETs), field-effect transistors (FETs), and even graphene-based memory.[4−6]

Although single-crystal graphene is metallic (unable to confine electrons electrostatically), it can become semiconducting when produced in a narrow ($\leq$10 nm) ribbon-like geometry, a manifestation of electronic quantum confinement.[1] However, the physical properties of nanoscale graphene devices are predicted to be strongly affected by the edges, which act as defects in graphene's crystal structure.[7−9] Recent studies of the transport properties of graphene nanoribbon based FET architectures revealed the strong impact of edge states for nanoribbons having widths below 50 nm.[10] Therefore, it is important to understand the symmetry breaking nature of the edges and associated local electronic effects.

In this work, we use Raman spectroscopy to experimentally study the coherence length of photoexcited charge carriers near the edges of graphene, where electrons or holes undergo inelastic scattering with optical phonons and elastic scattering with the edges. Using a novel optical defocusing method, we measure the localization l_D of the disorder-induced Raman D band ($\sim$1350 cm^{-1})[11] with a resolution of a few nanometers. We have performed temperature-dependent measurements of D band scattering near the edges of graphene. As the temperature is decreased from 300 to 1.55 K, the length l_D increases. Our measurements reveal that the localization of the D band varies as $1/T^{1/2}$, giving strong evidence that l_D scales with the coherence length of photoexcited electrons and holes near graphene edges.

Figure 1 shows the schematic of the experimental setup. The sample was placed into a helium bath cryostat capable of operating from 300 to 1.55 K, where the lowest temperatures were achieved by submerging the sample in superfluid helium. The sample was excited using a 532 nm laser line. The illumination and collection were accomplished through the same objective and the signal was sent to either an avalanche photodiode (APD) or a spectrometer with a charge coupled device (CCD). An $x-y$ piezo scan-stage was used for sample positioning, as well as confocal imaging. The scan stage was calibrated at each temperature using the width of the graphene flake obtained from topography measurements.

The objective used in the cryostat was a commercially available aspheric lens (NA_{asph} = 0.55) in conjunction with an aplanatic *numerical aperture increasing lens* (NAIL) that was bonded to the fused silica (n = 1.45) substrate.[12] The NAIL material was chosen to be fused silica to index match the coverslip, eliminating reflections from the interface. The numerical aperture with the NAIL is described by: $NA_{NAIL} = n^2\, NA_{asph}$, leading to $NA_{NAIL} \approx$ 1.1 and a resolution improvement of approximately 2.[12] However, due to the chromatic aberrations of the aspheric objective,

Received: November 27, 2010
Revised: January 26, 2011
Published: February 22, 2011

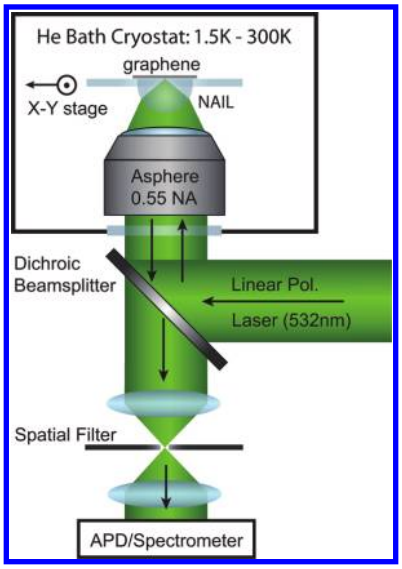

Figure 1. Schematic of the experimental setup. The sample was placed into a helium bath cryostat (1.55−300 K). The illumination and collection were accomplished through an aspheric lens combined with a NAIL that was bonded to the fused silica substrate. The signal was sent to either an APD or a spectrometer. An $x-y$ piezo scan-stage was used for confocal imaging and sample positioning.

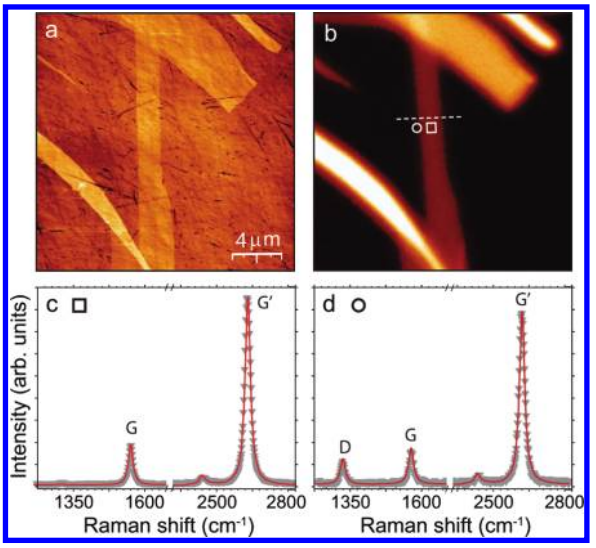

Figure 2. (a) Topographic image of exfoliated graphene deposited on a fused silica substrate. (b) Confocal Raman image showing the intensity of the G band over the same region. The dashed line indicates the direction along which Raman scattering spectra were recorded. (c, d) Raman spectra evaluated at the locations indicated by the square and circle in (b). The D band shows up only at the graphene edge. Spectrum d was scaled by a factor of 3 relative to spectrum c.

the actual resolution of the system corresponds to an NA closer to 0.8. Chromatic aberration was compensated by using confocal detection for both the spectrometer and APD. In the detection path we incorporated a spatial filter to maximize the spatial resolution for the D and G (1580 cm^{-1}) bands. Because the D and G bands are spectrally close (~7 nm), the difference in chromatic aberration between these bands is negligible.

Figure 2a shows a topographic image recorded by atomic force microscopy (AFM) of a set of graphene pieces deposited on a fused silica surface. A corresponding confocal Raman image of the same region is depicted in Figure 2b. The contrast (color scale) in the Raman image renders the intensity of the bond-stretching G band. The G band is a first-order scattering process that originates from the double-degenerate vibrational mode Γ_6^+ (E_{2g}) that occurs at the crossing of the longitudinal optical (LO) and transverse optical (TO) phonon branches at the Γ point in the first Brillouin zone of graphene.[11] Panels c and d of Figure 2 show full Raman scattering spectra acquired at two different locations indicated by the white square and circle in Figure 2b. Spectrum c was acquired from the interior of the graphene piece (≈1 μm from the edge), whereas spectrum d was recorded with the incident laser focus centered at the left edge. Spectrum c shows two major Raman features: the G band and the G′ band (also called 2D band) centered at ~2700 cm^{-1}. The G′ band originates from two-phonon Raman processes involving TO phonons[13] whose wavevectors extend next to the corner of the first Brillouin zone (K and K' points). The single-Lorentzian shape of the G′ band indicates that the measured sample region is indeed a single-layer graphene piece.[14]

Both G and G′ bands are also detected in the Raman spectrum of Figure 2d (obtained from the edge). In addition to the peaks identified in the previous spectrum, we now also observe the defect-induced D band.[11] Due to momentum conservation, the TO phonons giving rise to this band only become Raman active if the electrons or holes involved in the scattering process undergo elastic scattering by a lattice defect,[15] which in this case is provided by the graphene edge.[16−19] Therefore, the closer the position of a photogenerated electron−hole pair to the graphene edge, the higher is its probability that electron or hole will be involved in D band scattering. Notice that although the G′ band is the overtone of the D band, it does not require the presence of defects to become Raman active, since momentum conservation is guaranteed in two-phonon Raman processes. The Raman spectra shown in Figure 2c,d were recorded with the polarization vector of the excitation laser beam oriented parallel to the graphene edge, since polarizations perpendicular to the edge do not generate D band scattering.[16,18]

In order to analyze the spatial dependence of the D, G, and G′ intensities, we have recorded Raman scattering spectra for different positions of the laser focus relative to the graphene edge. The incident beam was moved in steps of 100 nm along a 5 μm long line perpendicular to the edges of a narrow graphene piece (dashed line in Figure 2b). Figure 3a shows a hyperspectral Raman map recorded along the scan line. The horizontal axis refers to the spatial position of the incident laser (in micrometer units) and the vertical axis renders the Raman shift. As the graphene piece is stepped through the laser focus, the intensities of the G and G′ bands gradually transition from a minimum value (dark counts) to a maximum value. On the other hand, the D band intensity achieves a maximum value when the graphene edge is in the laser focus. Figure 3b and Figure 3c show the intensity profile of the D and G bands, respectively, obtained from the hyperspectral data shown in panel a.

Because the intensity profile of the incident laser beam corresponds to a finite point-spread function (PSF), the intensity profiles shown in Figure 3 originate from the spatial convolution of the Raman material response with the strength of the incident electric field. Initial attempts to determine the spatial confinement l_D of the D band have been made by making use of prior information about the PSF of a strongly focused beam.[17] This prior knowledge was used to deconvolve the D band confinement

dx.doi.org/10.1021/nl104134a |*Nano Lett.* 2011, 11, 1177–1181

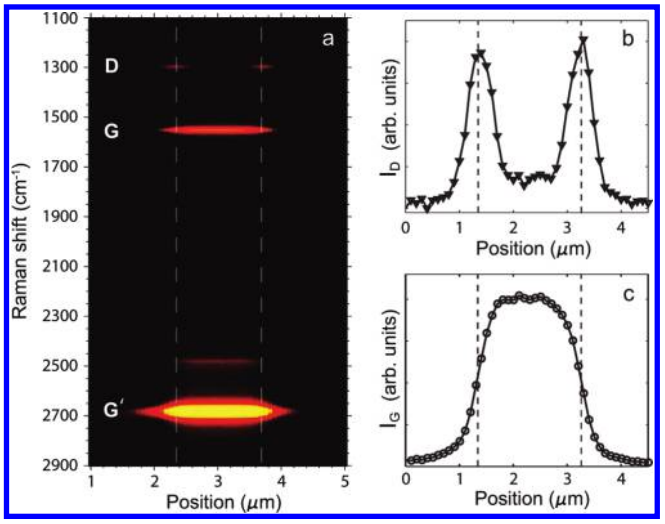

Figure 3. (a) Hyperspectral line scan recorded along the dashed line in panel b of Figure 2. The vertical lines indicate the position of the edges of the graphene piece. The D band is localized at the graphene edges. (b, c) Intensity profiles of the D and G bands obtained from the hyperspectral data shown in (a).

from the recorded scan profile across a graphene edge. However, this method was only able to provide an upper limit of about 20 nm[17] and is not accurate enough to quantitatively determine the D band confinement. To overcome previous limitations, we here introduce a defocusing technique to extract l_D from the ratio of G and D band intensities.

When the laser focus is centered at the edge of the graphene piece, the G band intensity (I_G) is proportional to the area of the laser focus, whereas the D band intensity is zero in the absence of defects. D band scattering can be observed once the laser focus is placed near a graphene edge, which serves as a one-dimensional model defect. As depicted in Figure 4a, the D band intensity (I_D) is proportional to the area defined by the spatial D band confinement l_D (measured from the edge) and the length of the graphene edge exposed to the incident laser beam. Hence, the intensity ratio I_G/I_D turns out to be proportional to the full width at half-maximum (FWHM) of the point-spread function. For a Gaussian focus of width σ, this result can be formally derived as

$$I_G \propto \int_0^{\infty}\int_{-\infty}^{\infty} \chi_G^2\, e^{-\frac{(x^2+y^2)}{2\sigma^2}}\, dy\, dx = \pi\chi_G^2\sigma^2 \qquad (1)$$

$$I_D \propto \int_0^{l_D}\int_{-\infty}^{\infty} \chi_D^2\, e^{-\frac{(x^2+y^2)}{2\sigma^2}}\, dy\, dx \cong \sqrt{2\pi} l_D \chi_D^2 \sigma \qquad (2)$$

where the lateral position of the edge is fixed at $x = 0$ (see Figure 4a for reference). χ_G and χ_D are the Raman material response of the G and D bands, respectively. Notice that we have considered $l_D \ll \sigma$ in (2). The ratio I_G/I_D obtained from (1) and (2) for the focus centered at the edge gives

$$\frac{I_G}{I_D} = \frac{1}{4}\sqrt{\frac{\pi}{\ln(2)}}\frac{\chi_G^2}{\chi_D^2}\frac{\Delta}{l_D} \qquad (3)$$

where we have used the relation $\sigma = \Delta/[(2\ln(2))^{1/2}]$, with Δ being the FWHM. χ_G^2/χ_D^2 is the ratio between the strengths of the G and D bands in graphene.

The ratio χ_G^2/χ_D^2 has been empirically determined in recent work by Lucchese et al. by measuring the I_D/I_G ratio in graphene samples with point defects produced by ion bombardment.[20] Using the measured I_D/I_G ratio in combination with a phenomenological model leads to a value of χ_G^2/χ_D^2 between 0.24 and 0.28.[20] Note, however, that the study of Lucchese et al. dealt with point defects and not with linear defects (edges) as in the case of our experiments. Edges introduce chirality differences and a dependence on polarization.[16,18,19] Despite theses differences, ref 20 provides the best available estimate for the χ_G^2/χ_D^2 ratio, although additional work is required to understand how the material response depends on defect type and edge chirality.

According to (3), the plot of the ratio I_G/I_D versus Δ gives a line whose slope is proportional to l_D. Therefore, the width l_D can be experimentally determined by performing several line scans with different amounts of defocus, which means different Δ values. Since $l_D \ll \sigma$, as shown in ref 17, the spatial profile of the D band is a good approximation to the line response function of the focus and can be used as a direct measurement of Δ. The ratio $I_D/I_{G_{Max}}$ for different amounts of defocus is shown in Figure 4b, where $I_{G_{Max}}$ is the I_G value taken from the center of the sample. Figure 4c shows the plot I_G/I_D versus Δ for the experimental data obtained using this technique at room temperature. The linear fit (solid line) gives $I_G/I_D = 42\ \mu m^{-1}\ \Delta$, which according to (3) leads to $l_D \approx 3$ nm, using the empirical model from ref 20. This is in excellent agreement with recent work by Lucchese et al. where the authors have measured a D band relaxation length of ≈3 nm for point defects.[20]

In order to investigate the connection between the spatial localization of the D band and the transport properties of electrons near graphene edges, we have collected Raman scattering spectra for temperatures ranging from 1.55 to 300 K. In Figure 5a we plot the ratio $I_D/I_{G_{Max}}$ for different values of temperatures along the scan line indicated in Figure 2b. The experimental data show that the ratio increases as the temperature decreases (cf. Figure 5a), indicating that the D band scattering length is increasing. This result provides clear evidence for D band delocalization at low temperatures. To quantify the experimental data, we have recorded the temperature dependence of l_D by repeating the defocusing experiment in Figure 4c for different temperatures. The results are shown in Figure 5b, which depicts l_D as a function of inverse sample temperature for both edges. The dashed line is a linear fit showing that $l_D \propto 1/T^{1/2}$.

The electron coherence length, also called phase-breaking length L_ϕ, is defined as the average distance traveled before undergoing inelastic scattering.[21,22] Since electrons or holes involved in D band Raman scattering undergo a single inelastic scattering event with a lattice phonon, the average distance l_D traveled by electrons or holes during the time interval in which the D band scattering process takes place should be proportional to L_ϕ. It is well-known that the phase-breaking length increases as the temperature decreases.[22] More specifically, recent low temperature transport experiments have shown that the phase breaking length of charge carriers in graphene is proportional to $1/T^{1/2}$,[23] which is the same trend followed by l_D as shown in Figure 5b.

A recent work[18] has explained that for *any* one-phonon Raman scattering process (such as D band scattering) the relaxation length is associated with the virtual electron−hole pair lifetime. The authors argued that since the energy uncertainty in such a process is determined by the phonon energy ω_{ph}, the minimum value for the electron−hole pair lifetime obtained from the uncertainty principle is $1/\omega_{ph}$. By using the relation v/ω_{ph}, where v is the group velocity of the photoexcited electrons, the

dx.doi.org/10.1021/nl104134a |*Nano Lett.* 2011, 11, 1177–1181

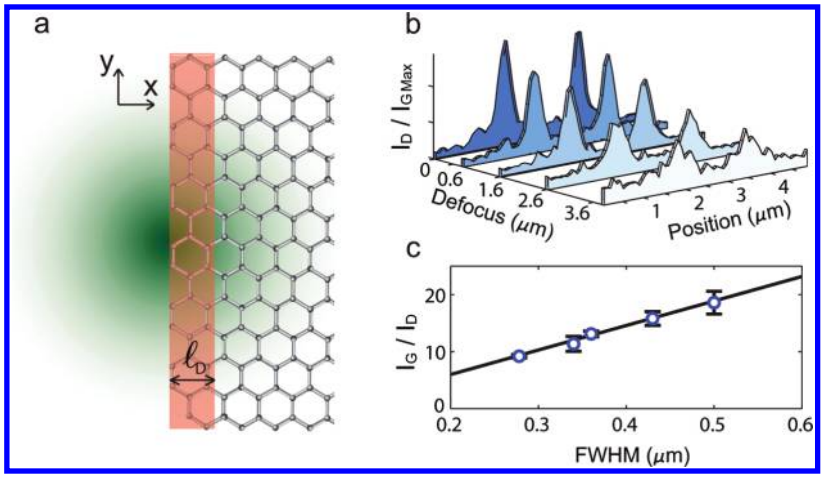

Figure 4. (a) Sketch of the measurement technique. The laser focus is scanned across the graphene edge along the x direction. The light red rectangle indicates the region in which the D band signal is generated. (b) Line scan profile for the ratio $I_D/I_{G_{Max}}$ obtained along the dashed line shown in Figure 2a for different amounts of defocus. (c) Plot of the experimental data of the ratio I_G/I_D as a function of Δ. The solid line is a linear fit giving $I_G/I_D = 42\ \mu m^{-1}\ \Delta$.

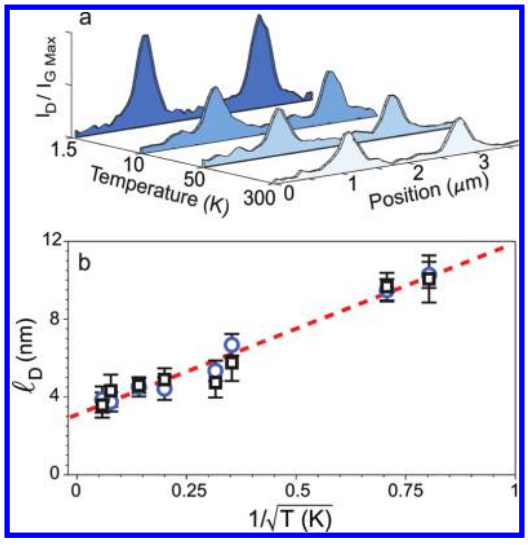

Figure 5. (a) Line scan profile for the ratio $I_D/I_{G_{Max}}$ along the dashed line in Figure 2b evaluated for different temperatures. (b) Plot of l_D as a function of $1/T^{1/2}$ for the left edge (blue circles) and the right edge (black squares) of the graphene sample. The dashed line shows a linear fit giving l_D (nm) = $3 + 9/T^{1/2}$.

authors have found $l_D \approx 4$ nm. The linear fit in Figure 4b yields l_D(nm) = $3 + 9/T^{1/2}$, with a limiting value of l_D = 3 nm for high temperatures ($T \geq 300$ K). This result indicates that the value estimated for l_D in ref 18 corresponds to a lower limit determined by the uncertainty principle. This limit is accurate for high-temperature regimes.

Low-temperature transport measurements in graphene have provided values for the phase breaking on the order of 1 μm,[23,24] which is about 2 orders of magnitude larger than the l_D values reported here. However, our method probes *photoexcited* electrons and holes, whose energy is more than a hundred times larger than the energy of charge carriers involved in transport measurements. As discussed in ref 18, the phase-breaking length of electrons or holes that undergo inelastic scattering with TO phonons near the K point in the first Brillouin zone of graphene can be estimated to be about 10 nm, based on the values of the electron−phonon scattering rate provided by recent literature data.[25−27] This value is in good agreement with the values obtained in our low temperature experiments. Moreover, the coherence length measured here provides a route for studying transport properties of narrow graphene nanorribons, which exhibit relatively large energy gaps (on the order of 0.5 eV) due to the quantum confinement.[9,28−30]

In summary, we have introduced a novel optical defocusing method for the measurement of the spatial confinement and temperature dependence of localized states, such as D band Raman scattering. Our measurements yield a D band confinement of l_D = 3 nm at T = 300 K and a temperature dependence of $1/T^{1/2}$, which indicates that l_D scales with the coherence length of photoexited electrons or holes that undergo inelastic scattering by optical phonons. This work demonstrates a strong connection between electronic and optical properties of graphene and shows that Raman spectroscopy provides an alternative tool for studying electric transport in mesoscopic structures.

AUTHOR INFORMATION

Corresponding Author

*E-mail: novoty@optics.rochester.edu.

ACKNOWLEDGMENT

The authors thank C. Höppener, B. Deutsch, P. Bharadwaj, and A. Jorio for valuable discussions and input. This work was supported by the Department of Energy (Grant DE-FG02-05ER46207).

REFERENCES

(1) Avouris, Ph.; Chen, Z.; Perebeinos, V. *Nat. Nanotechnol.* **2007**, *2*, 605–615.
(2) Castro-Neto, A. H. *Mater. Today* **2010**, *13*, 12–17.
(3) Geim, A. K.; Novoselov, K. S. *Nat. Mater.* **2007**, *6*, 183.
(4) Stampfer, C.; Schurtenberger, E.; Molitor, F.; Güttinger, J.; Ihn, T.; Ensslin, K. *Nano Lett.* **2008**, *8*, 2378–2383.
(5) Meric, I.; Han, M. Y.; Young, A. F.; Ozyilmaz, B.; Kim, P.; Shepard, K. L. *Nat. Nanotechnol.* **2008**, *3*, 654–659.
(6) Li, Y.; Sinitskii, A.; Tour, J. M. *Nat. Mater.* **2008**, *7*, 966–971.
(7) Louis, E.; Vergés, J. A.; Guinea, F.; Chiappe, G. *Phys. Rev. B* **2007**, *75*, No. 085440.

(8) Areshkin, D. A.; Gunlycke, D.; White, C. T. *Nano Lett.* **2007**, *7*, 204.
(9) Ritter, K. A.; Lyding, J. W. *Nat. Mater.* **2009**, *8*, 235–242.
(10) Chen, Z.; Lin, Y. M.; Rooks, M. J.; Avouris, Ph. *Physica E* **2007**, *40*, 228.
(11) Tuinstra, F.; Koenig, J. L. *J. Chem. Phys.* **1970**, *53*, 1126–1130.
(12) Ippolito, S. B.; Goldberg, B. B.; Ünlü, M. S. *J. Appl. Phys.* **2005**, *97*, 053105.
(13) Ferrari, A. C.; Robertson, J. *Phys. Rev. B* **2001**, *64*, No. 075414.
(14) Ferrari, A. C.; Meyer, J. C.; Scardaci, V.; Casiraghi, C.; Lazzeri, M.; Mauri, F.; Piscanec, S.; Jiang, D.; Novoselov, K. S.; Roth, S.; Geim, A. K. *Phys. Rev. Lett.* **2006**, *97*, No. 187401.
(15) Thomsen, C.; Reich, S. *Phys. Rev. Lett.* **2000**, *85*, 5214.
(16) Cançado, L. G.; Pimenta, M. A.; Neves, B. R. A.; Dantas, M. S. S.; Jorio, A. *Phys. Rev. Lett.* **2004**, *93*, No. 247401.
(17) Cançado, L. G.; Beams, R.; Novotny, L. Preprint at http://arxiv.org/abs/0802.3709, 2008.
(18) Casiraghi, C.; Hartschuh, A.; Qian, H.; Piscanec, S.; Georgi, C.; Fasoli, A.; Novoselov, K. S.; Basko, D. M.; C.Ferrari, A. *Nano Lett.* **2009**, *9*, 1433–1441.
(19) Krauss, B.; Nemes-Incze, P.; Skakalova, V.; Biro, L. P.; vonKlitzing, K.; Smet, J. H. *Nano Lett.* **2010**, *10*, 4544–4548.
(20) Lucchese, M. M.; Stavale, F.; MartinsFerreira, E. H.; Vilahn, C.; Moutinho, M. V. O.; Capaz, R. B.; Achete, C. A.; Jorio, A. *Carbon* **2010**, *48*, 1592–1597.
(21) Taylor, P. L.; Heinonen, O. A. *Quantum Approach to Condensed Matter Physics*; Cambridge University Press: Cambridge, U.K., and New York, 2002.
(22) Beenakker, C. W. J.; vanHouten, H. *Solid State Phys.* **1991**, *44*, 1–228.
(23) Morozov, S. V.; Novoselov, K. S.; Katsnelson, M. I.; Schedin, F.; Ponomarenko, L. A.; Jiang, D.; Geim, A. K. *Phys. Rev. Lett.* **2006**, *97*, No. 016801.
(24) Kechedzhi, K.; Horsell, D. W.; Tikhonenko, F. V.; Savchenko, A. K.; Gorbachev, R. V.; Lerner, I. V.; Fal'ko, V. I. *Phys. Rev. Lett.* **2009**, *102*, No. 066801.
(25) Piscanec, S.; Lazzeri, M.; Mauri, F.; Ferrari, A. C.; Robertson, J. *Phys. Rev. Lett.* **2004**, *93*, No. 185503.
(26) Basko, D. M.; Aleiner, I. L. *Phys. Rev. B* **2008**, *77*, No. 041409(R).
(27) Lazzeri, M.; Attaccalite, C.; Wirtz, L.; Mauri, F. *Phys. Rev. B* **2008**, *78*, No. 081406(R).
(28) Han, M. Y.; Özyilmaz, B.; Zhang, Y.; Kim, P. *Phys. Rev. Lett.* **2007**, *98*, No. 206805.
(29) Li, X.; Wang, X.; Zhang, L.; Lee, S.; Dai, H. *Science* **2008**, *319*, 1229–1232.
(30) Dubois, S. M. M.; Zanolli, Z.; Declerck, X.; Charlier., J. C. *Eur. Phys. J. B* **2009**, *72*, 1–24.